Available online at www.sciencedirect.com
ScienceDirect
Journal of Bionic Engineering 11 (2014) 188–198

Control of a Quadruped Robot with Bionic Springy Legs in Trotting Gait

Mantian Li[1], Zhenyu Jiang[1], Pengfei Wang[1], Lining Sun[1], Shuzhi Sam Ge[2,3]

1. *State Key Laboratory of Robotics and System*, *Harbin Institute of Technology*, *Harbin* 150001, *P. R. China*
2. *Institute of Intelligent Systems and Information Technology*, *University of Electronic Science and Technology of China*, *Chengdu* 610000, *P.R. China*
3. *Department of Electrical and Computer Engineering*, *the National University of Singapore*, *Singapore* 117576, *Singapore*

Abstract

Legged robots have better performance on discontinuous terrain than that of wheeled robots. However, the dynamic trotting and balance control of a quadruped robot is still a challenging problem, especially when the robot has multi-joint legs. This paper presents a three-dimensional model of a quadruped robot which has 6 Degrees of Freedom (DOF) on torso and 5 DOF on each leg. On the basis of the Spring-Loaded Inverted Pendulum (SLIP) model, body control algorithm is discussed in the first place to figure out how legs work in 3D trotting. Then, motivated by the principle of joint function separation and introducing certain biological characteristics, two joint coordination approaches are developed to produce the trot and provide balance. The robot reaches the highest speed of 2.0 $m{\cdot}s^{-1}$, and keeps balance under 250 $Kg{\cdot}m{\cdot}s^{-1}$ lateral disturbance in the simulations. The effectiveness of these approaches is also verified on a prototype robot which runs to 0.83 $m{\cdot}s^{-1}$ on the treadmill. The simulations and experiments show that legged robots have good biological properties, such as the ground reaction force, and spring-like leg behavior.

Keywords: legged robots, locomotion control, quadruped robot, trotting gait

doi: 10.1016/S1672-6529(14)60043-3

1 Introduction

Modeling and control of legged robots has long been a challenging issue in the control community and can be traced back to the 1960s. One of the advantages of legged locomotion is that legged robots usually tolerate much larger discontinuities in the terrain than that of wheeled robots. Among legged robots, a widely investigated class is the quadruped robot, which is expected as an attractive machine for transportation in a complex environment. The quadruped presents a rich set of running gaits such as trot, pace and bound. It has shown that trot is the most preferred gait for the quadruped robots from the viewpoint of high speed, energy efficiency and ground adaptability.

An extensive literature is currently available on the issues of quadruped robots such as modeling, adaptive gait pattern control, gait transition, and learning locomotion. Based on the model of Spring-Loaded Inverted Pendulum (SLIP) and the concept of virtual leg, Raibert *et al*.[1–3] reported that the three-part control algorithm used for one-legged running robots was generalized to the quadruped running. The dynamic properties of SLIP system are similar to the behaviors of real animals. Therefore, SLIP or other simplified models developed from SLIP were widely used in legged robot research. Based on a sagittal model, Scout II quadruped robot could achieve dynamically stable running[4]. The pronking gait of a two-legged robot was also studied in Ref. [5], which implied that the control of touchdown angle is sufficient to stabilize the pitch motion. However, these simplified models usually could not describe more dynamics details in quadruped robot, such as the 6 Degrees of Freedom (DOFs) of rigid body in legged robot. Palmer *et al*.[6–8] built a quadruped robot and used fuzzy control techniques to achieve the running in simulation environment. It is worth pointing out that in Ref. [8], a control algorithm was proposed to fulfill high-speed banked turn by putting the leg crabwise. Virtual Model Control (VMC) is an intuitive method to control the legged robot,

Corresponding author: Pengfei Wang
E-mail: wangpengfei1007@163.com

which was firstly proposed by Pratt *et al*. to control the bipedal robot[9]. Hutter *et al*. also used the VMC to control 2D running[10]. These methods could be enlightened in the attitude control of legged robot in dynamic walking. But another challenge is how to control the leg with multi-joints and redundant actuations. Researches have also been done on a control system based on the principles taken from neurobiology. The Central Pattern Generator (CPG) imitates the nerve system of the animal and coordinates all joints to complete a movement[11–15]. Wang *et al*. employed a bio-inspired neural mechanism to control each "muscle" in leg[16]. However, we expect to develop a four-legged robot which has similar structure and dynamic behaviors to animal.

The biological characteristics of trotting quadrupeds were explored[17–20]. Lee *et al*.[18] found that there were certain special landing patterns for the trotting dog. In addition, it is shown in Ref. [20] that the forward-point elbow and rear-point knee of quadruped mammals could efficiently weaken the fluctuation of the pitch motion. Krasny *et al*. built a quadruped model with biological characteristics and considered the 3D gallop gait, in which nearly the entire cycle was spent in flight phase[21]. It seems that introducing biological characteristics into robots may simplify the control design and improve the performance significantly.

This paper addresses the problem of trotting control of a quadruped robot with bionic springy legs. The goals are to enhance the robustness of trotting of a quadruped robot and to see if the quadruped running could be smoother and more stable by introducing certain biological characteristics. The rest of the paper is organized as follows. Section **2** describes the quadruped model with springy legs. Section **3** presents the approach of regulating the body motion, which makes the quadruped robot trot. In section **4**, two algorithms of coordinating the joints are given to achieve the body motion regulation. Sections **5** and **6** describe the implementation that is used to test the control algorithms in 3D simulation and experiment. Conclusion is given in section **7**.

2 Quadruped model

The 3D quadruped robot shown in Fig. 1 has four springy legs and a main body of 6 DOF. The control task is to make the quadruped robot trot, to propel the body in the desired direction at the desired speed, and to regulate the roll angle α_r, pitch angle α_p and yaw angle α_y, in the vicinity of zero point.

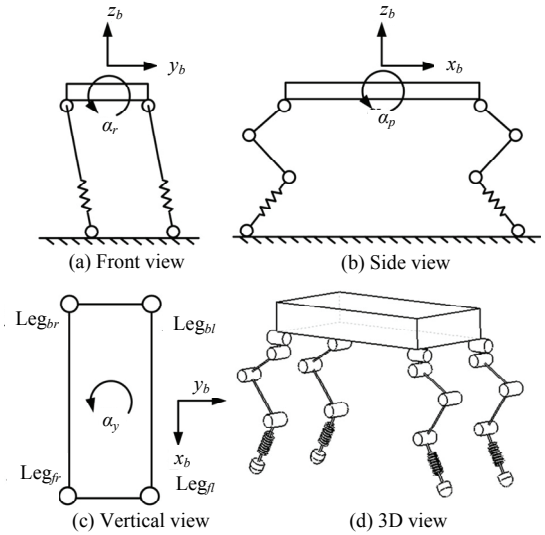

Fig. 1 Body model with simplified legs.

The leg is designed to imitate the mechanism of the leg of the mammal. As shown in Fig. 2, each leg consists of three links, and has four actuators (two at the hip, one at the knee, one at the ankle) and a total of 5 essential DOF (four rotational joints, one prismatic spring). The passive spring between the ankle joint and the foot is to replicate the elastic function of muscle and tendon in the leg of mammal, *i.e*. to store energy in stance phase and release it when lifting up.

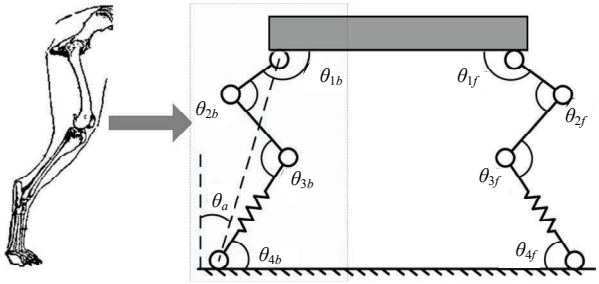

Fig. 2 Dynamic model of the robot in sagittal plane.

This nonlinear model with multi-DOF is the complete description of dynamic running. However, obtaining an accurate dynamic model for the quadruped robot is challenging due to the subtleties in the ground interactions, the dominant effects of motor saturations and transmission dynamics. In order to simplify the analysis of the model, the control for four-legged trotting is divided into two steps as follows.

3 Body control algorithm

Various control approaches have been proposed to fulfill the stable running of quadruped robots[2,7,14]. The body control algorithm is mainly based on the SLIP model, the characteristic of which is similar to the behavior of running mammal, and it is improved based on our previous work[22].

3.1 Control of SLIP model

Throughout the trotting cycle, the legs contact the ground under gravity and retract passively with the spring compressed from initial length. When the springs of the legs are in recovery state, the desired thrust is exerted on the legs to make the robot bounce. After one pair of diagonal legs lifts off the ground, it would retract instantly while the other pair would protract for landing. Since the trot gait uses the legs in diagonal pairs, based on the concept of virtual leg, the quadruped can be treated as an equivalent biped[2]. Based on the SLIP model as shown in Fig. 3, the body is connected with a springy leg. Assuming that the mass of the leg is negligible, the dynamics of the SLIP model is given by[22]

$$\begin{cases} M\ddot{r} + K(r - r_0) - Mr\dot{\theta}^2 = -Mg\cos\theta \\ \dfrac{d}{dt}(Mr^2\dot{\theta}) = Mgr\sin\theta \end{cases}, \quad (1)$$

where M is the weight of body, K is the elastic coefficient of spring, r is the length of leg, r_0 is the initial length of leg, and θ is the angle with respect to the vertical plane.

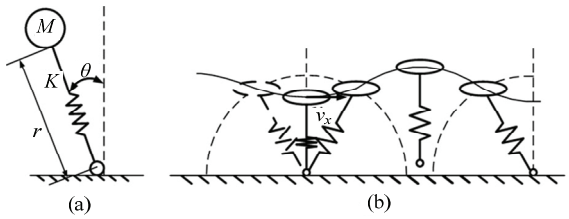

Fig. 3 Simplified model for forward and lateral running[22].

The control algorithm used to regulate running and hopping motions is similar to Raibert style[2], which is given by

$$\begin{cases} \theta_s = \arcsin\left(\dfrac{v_x T_s}{2l_0}\right) + k_p(v_x - v_{xt}) + k_i\sum_{step}(v_x - v_{xt}) \\ l_u = l_{u0} + C(v_z - v_{zt}) \end{cases}, \quad (2)$$

where θ_s is the given touch down angle, l_u is the given actuator length, T_s is the duration of stance phase, l_0 is the initial length of leg, v_x and v_z are the forward and vertical speed respectively, v_{xt} and v_{zt} are the target forward and vertical speed respectively, l_{u0} is the initial length of the actuator, k_p, k_i and C are constant parameters.

3.2 Control of forward, lateral running and yaw motion

Based on the control analyis of SLIP model, The forward and lateral running velocity of robot with straight legs[22] could be regulated by setting the forward and lateral touch angle on hip joints. The control of yaw motion can use the same approach. If one set of diagonal legs retracts and the other set protracts with certain opposite lateral touchdown angle, then the axial thrust of each leg will contribute to a moment such that the facing direction is steered. Considering that each leg of the robot works like a SLIP system, so the velocity of hip joints should be calculated firstly to select appropriate touch angles. The top view of the robot with straight legs is shown in Fig. 4.

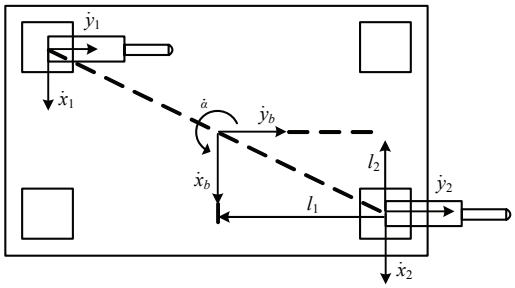

Fig. 4 The top view of the robot with straight legs.

Under the kinematics analysis, the forward and lateral velocities of hip joints are given by

$$\begin{cases} \dot{x}_1 = \dot{x}_b + \dot{\alpha}l_1 \\ \dot{y}_1 = \dot{y}_b - \dot{\alpha}l_2 \\ \dot{x}_2 = \dot{x}_b - \dot{\alpha}l_1 \\ \dot{y}_2 = \dot{y}_b + \dot{\alpha}l_2 \end{cases}, \quad (3)$$

where $\dot{x}_b$, $\dot{y}_b$, $\dot{\alpha}$ are the lateral, forward and yaw velocities of body respectively, $\dot{x}_i$ and $\dot{y}_i$ are the lateral and forward velocities of hip joints. The touch angles of hips to regulate three motions on body are given by

$$\begin{cases}\theta_{f\_touch1} = \arcsin\left(T_s(\dot{y}_b - \dot{\alpha}l_2)/2l_0\right) + \\ \qquad k_{yp}(\dot{y}_{bd} - \dot{y}_b) + k_{yi}\sum_{\text{step}}(\dot{y}_{bd} - \dot{y}_b) \\ \theta_{b\_touch1} = \arcsin\left(T_s(\dot{x}_b + \dot{\alpha}l_1)/2l_0\right) + \\ \qquad k_{xp}(\dot{x}_{bd} - \dot{x}_b) + \\ \qquad k_{yi}\sum_{\text{step}}(\dot{x}_{bd} - \dot{x}_b) + Yaw_{\text{feedback}} \\ \theta_{f\_touch2} = \arcsin\left(T_s(\dot{y}_b + \dot{\alpha}l_2)/2l_0\right) + \\ \qquad k_{yp}(\dot{y}_{bd} - \dot{y}_b) + k_{yi}\sum_{\text{step}}(\dot{y}_{bd} - \dot{y}_b) \\ \theta_{b\_touch2} = \arcsin\left(T_s(\dot{x}_b - \dot{\alpha}l_1)/2l_0\right) + \\ \qquad k_{xp}(\dot{x}_{bd} - \dot{x}_b) + \\ \qquad k_{yi}\sum_{\text{step}}(\dot{x}_{bd} - \dot{x}_b) - Yaw_{\text{feedback}}\end{cases}, \tag{4}$$

where, $\dot{x}_{bd}$ and $\dot{y}_{bd}$ are the target lateral and forward velocities on body, k_{yp}, k_{xp}, k_{yi} and k_{xi} are constant parameters. Yaw_{feedback} is the control input to regulate the yaw motion, which is given by

$$Yaw_{feedback} = K_{\gamma p}(\alpha_d - \alpha) + K_{\gamma d}(\dot{\alpha}_d - \dot{\alpha}), \tag{5}$$

where $\dot{\alpha}_d$ and $\dot{\alpha}$ are the target and actual yaw velocities on body, α_d and α are the target and actual yaw angles on body, $k_{\gamma p}$ and $k_{\gamma d}$ are constant parameters.

3.3 Pitching and rolling motions

As Raibert introduced the concept of "virtual leg", we can assume that the diagonal legs are coordinated to act in pairs. However, if the pitching or rolling angle is not zero, the diagonal legs cannot touch the ground simultaneously. The robot will fall down without the control of these two motions.

Note that the pitching and rolling motions could be described by a simplified model shown in Fig. 5. The dynamics is given by

$$J\ddot{\beta} = \tau_b + \tau_f + (F_2 - F_1)\cdot l_1/2, \tag{6}$$

where J is the rotational inertia of torso, β is the attitude angle, F_1 and F_2 are the contact forces of the feet, l_1 is the distance between two hip joint, τ_b and τ_f is the torque outputs of two hip joints.

Delighted by the VMC idea[9], we consider the body working as a spring-damper system. The control algorithm is given by

$$\begin{aligned} J\ddot{\beta} &= \tau_b + \tau_f + (F_2 - F_1)\cdot l_1/2 \\ &= \tau_x = -k_{p\beta}(\beta - \beta_d) - k_{d\beta}\dot{\beta}, \end{aligned} \tag{7}$$

where $k_{p\beta}$ is the stiffness, $k_{d\beta}$ is the damping in system. β_d is the expected attitude angle. Note that the model is a second order system, the transfer function is given by

$$\begin{aligned} \frac{\beta(S)}{\beta_d(S)} &= \frac{\omega_n}{S^2 + 2\xi\omega_n S + \omega_n{}^2} \\ &= \frac{2k_{p\beta}/J}{S^2 + 2k_{d\beta}S/J + 2k_{p\beta}/J}, \end{aligned} \tag{8}$$

where ξ and ω_n are the damping ratio and the natural frequency of the second order system respectively.

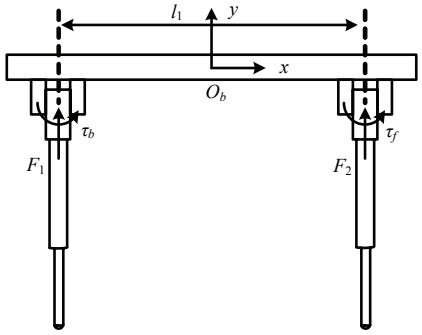

Fig. 5 Simplified model for rolling and pitching motion.

When the robot runs, the feet may all leave the ground. If the body has the initial angle velocity in the flight phase, the pitch and roll angles will be out of control. So these parameters should be chosen to make the attitude angle under control in stance phase. For example, according to the classical control theory, the setting time t_s with the step signal in second order system is given as

$$t_s = \frac{3.5}{\xi\omega_n}. \tag{9}$$

While, the duration of stance phase in this model is roughly equivalent to a half of oscillating period in spring-load system. To make the angle under control in stance phase, the setting time should be give by

$$t_s = a\pi\sqrt{\frac{m}{2K}}, \tag{10}$$

where K is the stiffness of leg, m is the weight of torso, a is the time ratio which is set to be 0.7 in our research.

To decrease the setting time and the overshoot, a damping ratio ξ is also needed in control of second order system, which is also set to be 0.7. Under these analyses, the control parameters of attitude angle are given by

$$\begin{cases} k_{d\beta} = 1.4J\sqrt{\dfrac{k_{ph}}{m}} \\ k_{p\beta} = \dfrac{k_{d\beta}^{\ 2}}{0.98J} \end{cases}. \tag{11}$$

4 Joint coordination algorithm

Since the leg has multi revolute joints, Joint Coordination Algorithm (JCA) is necessary. Noted that each joint in straight leg plays a different role in regulating different motions on torso when 3D trotting. Assigning particular function to each revolute joint in bionic leg may be an approach to solve this problem. Motivated by this thinking, we propose two JCAs.

4.1 JCA I

The function separation for JCA I is shown in Fig. 6. The main function of the hip joint is to displace the foot. The knee joint plays the role of generating the thrust when the robot lifts off and the ankle joint adjusts the touchdown angle of the passive spring such that θ_a, equals to $90^\circ-\theta_{4b}$ (in back leg) or $90^\circ-\theta_{4f}$ (in front leg) as shown in Fig 2. Take the back right leg for an example.

In flight phase, *i.e.* the contact force $F_{cbr} = 0$, the control algorithm is given by

$$\begin{cases} \theta_{0br} = \arcsin\left(T_s(\dot{x}_b + \dot{\alpha}l_1)/2r_1\right) + \\ \qquad k_{vxp}(\dot{x}_{bd} - \dot{x}_b) + \\ \qquad k_{vyi}\sum_{\text{step}}(\dot{x}_{bd} - \dot{x}_b) + Yaw_{\text{feedback}} \\ \theta_{1br} = \arcsin\left(T_s(\dot{y}_b - \dot{\alpha}l_2)/2r_1\right) + \\ \qquad k_{vyp}(\dot{y}_{bd} - \dot{y}_b) + k_{vyi}\sum_{\text{step}}(\dot{y}_{bd} - \dot{y}_b) \\ \theta_{2br} = C_2 \\ \theta_{3br} = C_3 \end{cases}, \tag{12}$$

where θ_{1br}, θ_{2br} and θ_{3br} are the angles shown in Fig. 2, θ_{0br} is the angle of lateral hip joint, k_{vxp}, k_{vyp}, k_{vxi}, k_{vyi}, C_2 and C_3 are constant parameters.

In stance phase, *i.e.* the contact force $F_{cbr} > 0$, the control algorithm is given by

$$\begin{cases} \tau_{0br} = k_{Rp}\gamma + k_{Rd}\dot{\gamma} \\ \tau_{1br} = k_{Pp}\beta + k_{Pd}\dot{\beta} \\ \theta_{2br} = \theta_{2br0} + C(\dot{z}_{bd} - \dot{z}_b) \\ \theta_{3br} = \pi - \\ \qquad \arcsin\left(\dfrac{l_{0br}\sin\theta_{2br}}{\sqrt{l_{0br}^{\ 2} + l_{1br}^{\ 2} - 2l_{0br}l_{1br}\cos\theta_{2br}}}\right) \end{cases}, \tag{13}$$

where τ_{0br} and τ_{1br} are the torques imposed on the hip joint to adjust the pitching and rolling motions, γ, β are the roll and pitch angle respectively, $\dot{z}_{bd}$, $\dot{z}_b$ are the target and actual vertical velocity on body, l_{0br} is the distance betwween hip and knee, l_{1br} is the distance betwween knee and ankle, k_{Rp}, k_{Rd}, k_{Pp}, k_{Pd} are constant parameters.

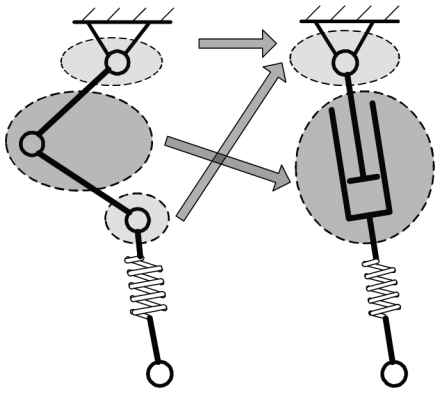

Fig. 6 Function separation in JCA I.

4.2 JCA II

There are some special skeleton configurations in mammals. For instance, as shown in Fig. 7, the orientation of the knee joint is opposite to that of the elbow joint. In stance phase, the fore leg tends to exert breaking force while the hind leg tends to exert propulsive force. It shows that there is an instinct connection between the biological characteristic and the balance.

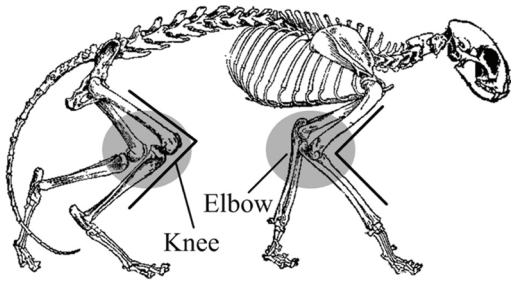

Fig. 7 Skeleton of a walking cat.

Fig. 8 shows the function of each joint for JCA II. The wrist and ankle joints are set to be opposite orientations to generate breaking or propulsive forces in stance phase. If the pitch angle and angle velocity are zero, the knee and elbow are the pure passive joints during the stance phase. The hip joint is used to generate thrust for another leap.

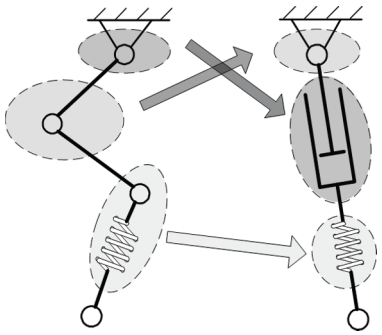

Fig. 8 Function separation in JCA II.

Due to the variation of the joint function, JCA II is slightly different from JCA I. Here we present JCA II for Leg$_{br}$. In flight phase, *i.e.* the contact force $F_{cbr} = 0$, the control algorithm is given by

$$\begin{cases} \theta_{0br} = \arcsin\left(T_s(\dot{x}_b + \dot{\alpha} l_1)/2r_1\right) + k_{vxp}(\dot{x}_{bd} - \dot{x}_b) + \\ \qquad k_{vyi}\sum_{\text{step}}(\dot{x}_{bd} - \dot{x}_b) + Yaw_{\text{feedback}} \\ \theta_{1br} = C_2 \\ \theta_{2br} = \arcsin\left(T_s(\dot{y}_b - \dot{\alpha} l_2)/2r_1\right) + k_{vyp}(\dot{y}_{bd} - \dot{y}_b) + \\ \qquad k_{vyi}\sum_{\text{step}}(\dot{y}_{bd} - \dot{y}_b) \\ \theta_{3br} = C_3 \end{cases}. \quad (14)$$

In stance phase, *i.e.* the contact force $F_{cbr} > 0$, the control algorithm is given by

$$\begin{cases} \tau_{0br} = k_{Rp}\gamma + k_{Rd}\dot{\gamma} \\ \theta_{1br} = \theta_{1br0} + C(\dot{z}_{bd} - \dot{z}_b) \\ \tau_{2br} = k_{Pp}\beta + k_{Pd}\dot{\beta} \\ \theta_{3br} = C_4 \end{cases}. \quad (15)$$

Remark: To keep the symmetry of the quadruped system, the forward placement of the fore- and hind foot with respect to the projection of each hip should be identical in flight phase. This condition requires the two dashed quadrangles shown in Fig.9 to be parallelograms.

Hence, the ankle and knees angles in JCA I should satisfy

$$\begin{cases} \psi_{1b} + \psi_{1f} = \pi \\ \theta_{2b} = \theta_{2f} \\ \theta_{3f} = \theta_{1f} - \psi_{1f} + \theta_{2f} \\ \theta_{3b} = \theta_{1b} - \psi_{1b} + \theta_{2b} \end{cases}. \quad (16)$$

While in JCA II, the joint angles should satisfy

$$\begin{cases} \psi_{2b} + \psi_{2f} = \pi \\ \theta_{1b} = \theta_{1f} \\ \theta_{3f} = \theta_{3b} \end{cases}, \quad (17)$$

where θ_{xb}, θ_{xf} are the angles shown in the Fig. 2.

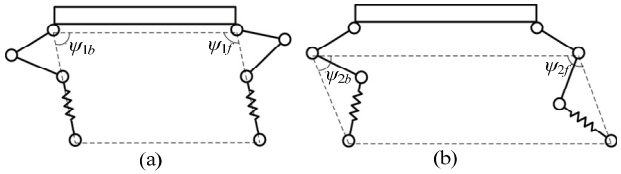

Fig. 9 The constraint to satisfy the symmetry. (a) JCA I, (b) JCA II.

5 Simulation and results

In this paper, the control algorithm is tested via co-simulation of ADAMS and Matlab/Simulink. The quadruped robot MBBOT was built in SolidWorks, as shown in Fig. 10. The parameters are given in Table I. The coefficient of ground spring is 10 MN·m^{-1}. The coefficient of kinetic friction between ground and feet is assumed being 0.9. The weight of robot is about 100 kg, which is close to the horse model (135 kg) used by McMahon[17]. He also found the stable trotting at 2.1 m·s^{-1} when the leg stiffness equaled to 24 KN·m^{-1}. In simulation, different values of stiffness are set close to 24 KN·m^{-1}, and 20 KN·m^{-1} is chosen at last.

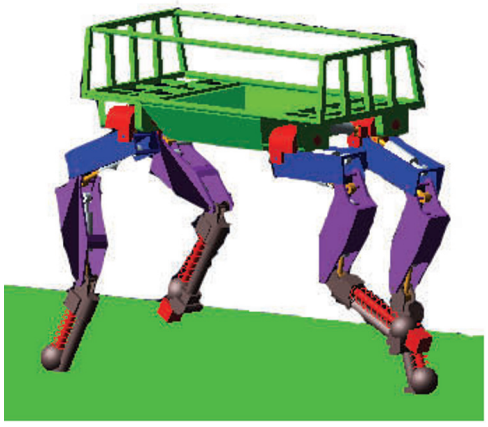

Fig. 10 Model of quadruped robot in simulations.

Table 1 Parameters list

Parameters	Value	Variable
M (kg)	67	Body mass
I_{xx} (kg·m^2)	1.75	Inertia around roll axis
I_{yy} (kg·m^2)	6.47	Inertia around pitch axis
I_{zz} (kg·m^2)	7.32	Inertia around yaw axis
L_{ss} (m)	0.3	Distance between two shoulders or hips
L_{sh} (m)	0.63	Distance between hip and shoulder
K (KN·m^{-1})	20	Spring stiffness
h (m)	0.85	Height of body COM
L_t (m)	0.233	Thigh length
L_s (m)	0.31	Shank length
L_f (m)	0.31	Foot length with spring in normal position
M_{th} (kg)	2.98	Thigh mass
M_s (kg)	2.32	Shank mass
M_f (kg)	2.09	Foot mass
M_{foe} (kg)	0.7	Toe mass

5.1 Simulation results of JCA I

The simulation results of JCA I are shown in Fig. 11. The forward running speed is regulated at 0.4 m·s^{-1}, and the lateral speed ranges from −0.2 m·s^{-1} to 0.1 m·s^{-1}. In addition, the pitching and rolling motions are well regulated. However, the robot would easily fall down when we tried to increase the desired running speed.

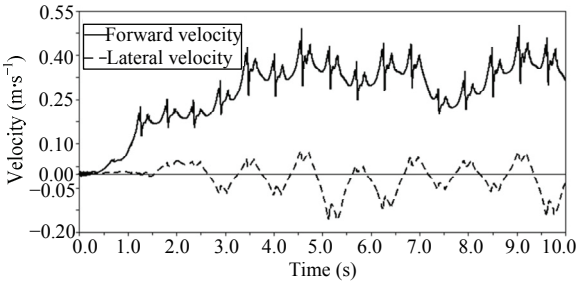

(a) The velocities of body in simulation

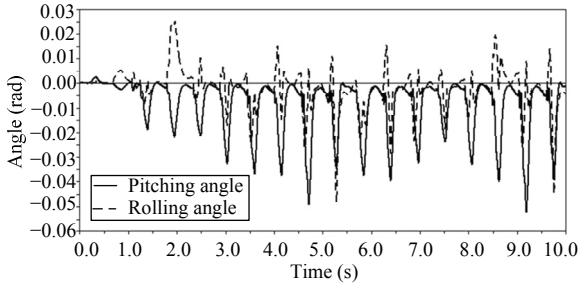

(b) The attitude angles of body in simulation

Fig. 11 The simulation results of JCA I.

5.2 Simulation results of JCA II

The simulation results of JCA II are presented in Fig.12. Compared with JCA I, the robot exhibits a higher running speed. In both JCA I and JCA II the legs are controlled to work like SLIP models. While, the distance between the hip joints of hind and fore legs is shorter than that of the keen joint in our model. By comparing the results of JCA I and JCA II, the longer distance of SLIP models may improve the stability of robot when trotting. On the other hand, the wrist and ankle joints are set to be opposite orientations to imitate the morphology of mammalians in JCA II, which may also efficiently weaken the fluctuation of the pitch motion[20]. These two reasons may explain why the robot with JCA II could run much faster and keep low fluctuation of pitch angle.

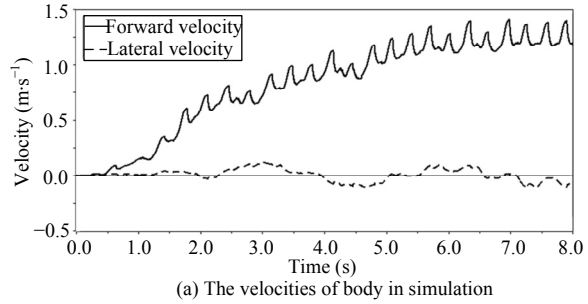

(a) The velocities of body in simulation

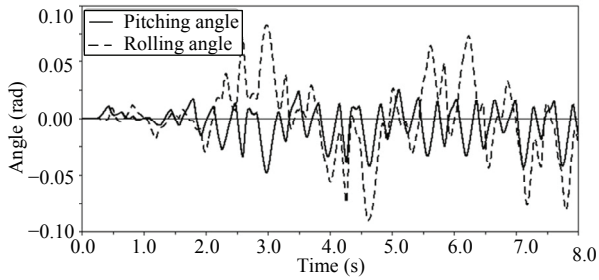

(b) The attitude angles of body in simulation

Fig. 12 The simulation results of JCA II.

The fore-aft force of a pair of diagonal feet is plotted in Fig. 13. The curves show that, the fore leg generates a breaking force while the hind leg generates a propulsive force in stance phase, which conforms to the mechanism of mammals. It may be another reason why the robot with JCA II can tolerate a stronger fluctuation of the pitch and roll angles.

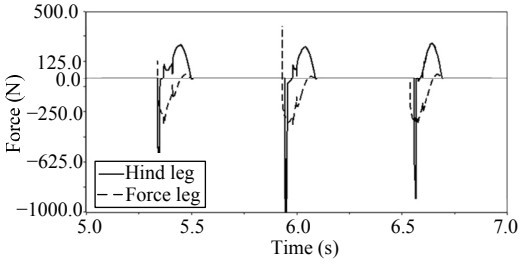

Fig. 13 The fore-aft force of legs.

However, the running speed of robot (1.5 m·s^{-1}) in simulation is still lower compared to that of animal. Introducing more energy into the system may be a solution to make the robot running fast. For mammalian, the energy could transfer between knee and ankle through the biarticular muscles of the shank[19,23]. In our model, there is no mechanism to realize the transfer of energy. However, the ankle and wrist joints could produce additional positive work by unbending these joints in stance phrase. Compared to the last simulations where the ankle/wrist joints stay still in stance phrase, the forward running speed goes to 2.0 m·s^{-1}, and the pitching and rolling motions are well controlled. The results are shown in Fig. 14.

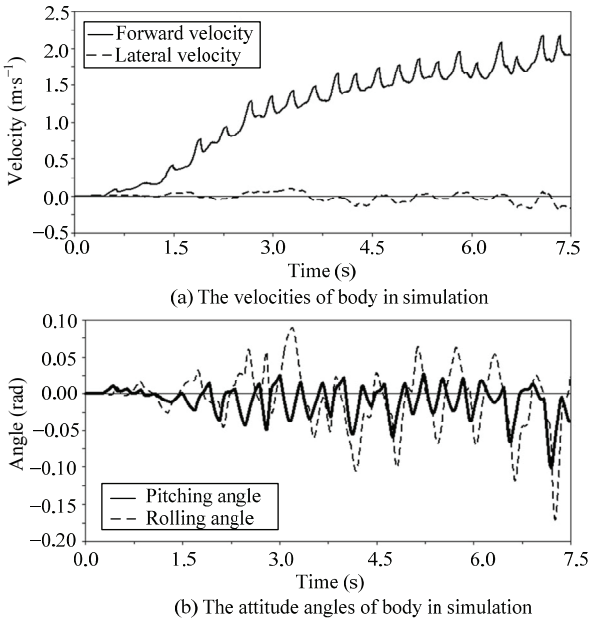

(a) The velocities of body in simulation

(b) The attitude angles of body in simulation

Fig. 14 The simulation results with higher running speed.

5.3 The performance under disturbance

The robustness of the control algorithm was discussed here. During the simulation, a lateral impulse force of 1000 N was exerted on the robot body COM for 0.25 s. As shown in Fig. 15, there was a strong fluctuation of the running motion at the very moment as the force was exerted. Because the impulse force was exerted on the lateral direction, there was a slight effect on the forward speed and the pitching motion. However, the lateral running speed and the rolling motion were seriously disturbed. In the result, the robot took three steps to keep stable, which verifies the validity of the control algorithm.

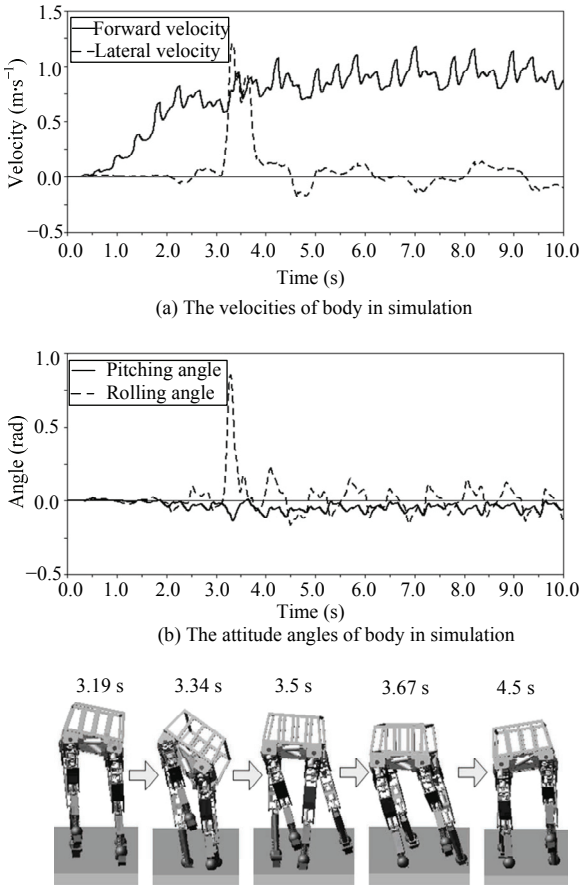

(a) The velocities of body in simulation

(b) The attitude angles of body in simulation

(c) Sequence of the trot under lateral disturbance in simulation

Fig. 15 The simulation results of the robot under lateral disturbances.

6 Experiment of prototype robot

To experimentally verify the control approach, the prototype of MBBOT is developed, which consists of one torso and four legs. Each leg has four active joints driven by four identical hydraulic cylinders, as well as a passive prismatic spring. All the actuators of 16 legs of the robot are powered by the external hydraulic pump. The robot has 41 sensors including displacement sensors and load cells on the hydraulic cylinders and springs, 3-component force sensors in feet and an Inertial Measurement Units (IMU) on torso. The velocity was estimated by robot kinematics.

A marking time trot was performed firstly to test the robot hardware and software. We did not install the battery or other payload on the robot, so the torso was almost empty. We pushed the torso of robot when it was stepping, as the red arrow shown in the first picture of Fig.16, and this lateral disturbance made the robot tend to roll and move laterally. The snapshots in Fig.16

show that the robot could keep stable under this disturbance. The blue quadrilateral is the marker on the ground. The time interval between two snapshots is about 250 ms.

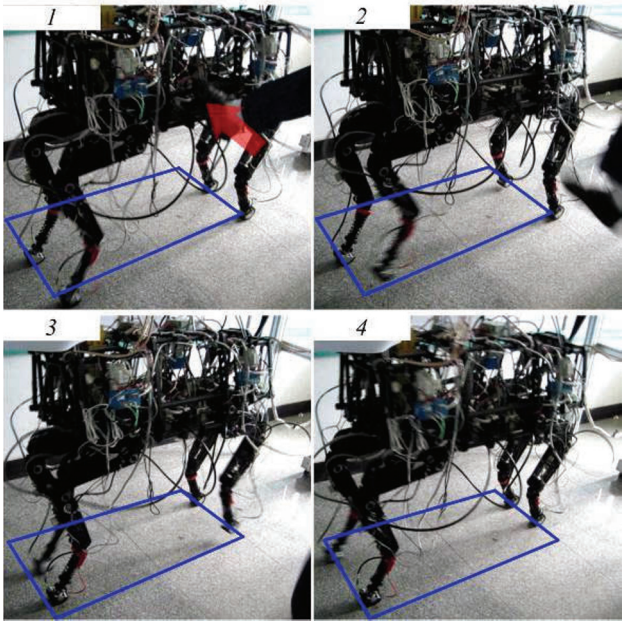

Fig. 16 Sequence of the marking time trot under lateral disturbance.

The trotting experiment was carried out on the treadmill. Fig.17 shows the snapshots in one trot cycle, where the small colored triangles mark the feet. The time interval between two snapshots is about 250 ms. As shown in Fig. 18a, the robot started to walk at 10 s, and took about 1 minute to accelerate to 0.83 $m \cdot s^{-1}$. The attitude angles were well regulated in walking as shown in Fig. 18b. Similar to the animal and the simulation result, the fore leg exerted breaking force while the hind leg exerted propulsive force, which is plotted in Fig. 18c. Because of the magnetic field excited by the motor in the treadmill, the yaw signal from the IMU drifted seriously. We had to compensate the target yaw angle by remote controller when robot was walking on 1.5 m width treadmill, so the yaw angle is not shown here. Because the robot with the power system and other payload weighs 200 kg, which is much higher than that of the model in simulations (100 kg), the prototype can not reach the high speed as shown in simulations presently. Our future work is to improve the design of mechanical system, especially to improve the performance of the actuators in legs.

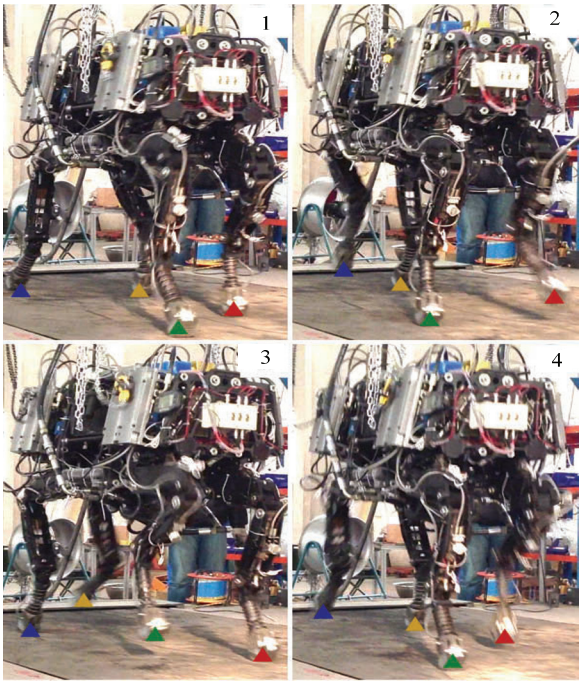

Fig. 17 Sequence of the trotting movement cycle.

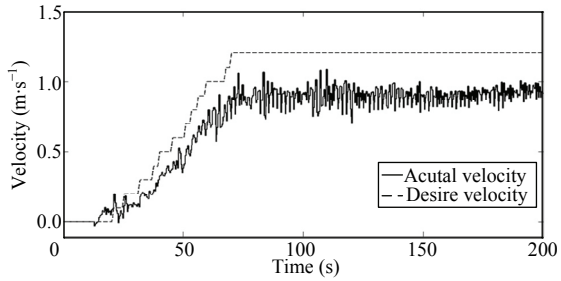

(a) The velocities of body when trotting on teadmill

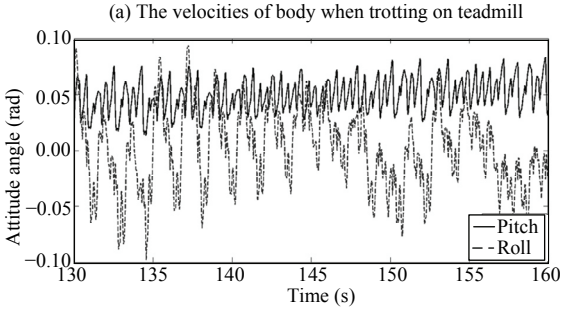

(b) The attitude angles of body when trotting on teadmill

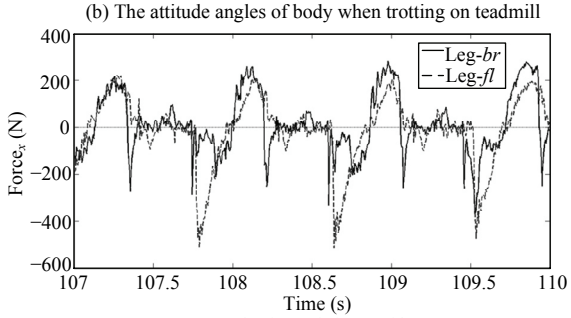

(c) The fore-aft force of legs

Fig. 18 The experiment results of prototype robot on treadmill.

7 Conclusion

In this paper, we have designed a quadruped robot with bionic springy legs. For this quadruped robot, a set of control algorithms based on SLIP model was given to regulate the forward and lateral running speed, hopping height, and body attitude. By the principle of joint function separation, two JCAs were established such that the quadruped robot could trot stably. The control strategies were tested by the simulations and experiments of the quadruped robot that trotted. We found that the robot with opposite orientations of ankle and wrist joint had the similar contact properties to the mammalian and could easily get higher running speed. Considering that energy could transfer between joints in mammalian, the robot speed up to 2 $m \cdot s^{-1}$ in the simulation by adding this function on ankle/wrist joints.

This paper preliminarily built the connection between the bionic trotting quadruped robot and the SLIP model by the control algorithm of the joints of leg which based on function separation. The results showed that the quadruped trotting could be smoother and more stable by absorbing certain biological characteristics.

The future work will be focused on (1) absorbing more biological characteristics, such as compliant joint and reflex actions, to improve the robot performance on challenging terrain and (2) optimizing the mechanical design of the robot on the basis of further simulation research and further analysis of animal motion.

Acknowledgment

This work was supported by the National Hi-tech Research and Development Program of China (863 Program, Grant No. 2011AA040701), and the National Natural Science Foundation of China (No. 61375097, No. 61175107)

References

[1] Raibert M H. *Legged Robots That Balance*. The MIT Press, Cambridge, Massachusetts, USA, 1986.

[2] Raibert M, Chepponis M, Jr Brown H. Running on four legs as though they were one. *IEEE Journal of Robotics and Automation*, 1986, **2**, 70–82.

[3] Raibert M H. Running with symmetry. *The International Journal of Robotics Research*, 1986, **5**, 3–19.

[4] Poulakakis I, Smith J A, Buehler M. Experimentally validated bounding models for the Scout II quadrupedal robot. *IEEE International Conference on Robotics and Automation*, New Orleans, USA, 2004, 2595–2600.

[5] Cherouvim N, Papadopoulos E. Pitch control for running quadrupeds using leg positioning in flight. *IEEE Mediterranean Conference on Control and Automation*, Athens, Greece, 2007, 1–6.

[6] Palmer L R, Orin D E. Force redistribution in a quadruped running trot. *IEEE International Conference on Robotics and Automation*, Roma, Italy, 2007, 4343–4348.

[7] Palmer L R, Orin D E. Attitude Control of a Quadruped Trot While Turning. *Proceedings of IEEE/RSJ International Conference on Intelligent Robots and Systems*, Beijing, China, 2006, 5743–5749.

[8] Palmer L R, Orin D E. Intelligent control of high-speed turning in a quadruped. *Journal of Intelligent and Robotic Systems*, 2010, **58**, 47–68.

[9] Pratt J, Chew C M, Torres A, Dilworth P, Pratt G. Virtual model control: An intuitive approach for bipedal locomotion. *The International Journal of Robotics Research*, 2001, **20**, 129–143.

[10] Hutter M, Remy C D, Hoepflinger M A, Siegwart R. ScarlETH: Design and control of a planar running robot. *IEEE/RSJ International Conference on Intelligent Robots and Systems*, San Francisco, USA, 2011, 562–567.

[11] Takemura H, Deguchi M, Ueda J, Matsumoto Y, Ogasawara T. Slip-adaptive walk of quadruped robot. *Robotics and Autonomous Systems*, 2005, **53**, 124–141.

[12] Inagaki S, Yuasa H, Suzuki T, Arai T. Wave CPG model for autonomous decentralized multi-legged robot: Gait generation and walking speed control. *Robotics and Autonomous Systems*, 2006, **54**, 118–126.

[13] Maufroy C, Nishikawa T, Kimura H. Stable dynamic walking of a quadruped robot "Kotetsu" using phase modulations based on leg loading/unloading. *IEEE International Conference on Robotics and Automation*, Anchorage, USA, 2010, 5225–5230.

[14] Spröwitz A, Tuleu A, Vespignani M, Ajallooeian M, Badri E, Ijspeert A J. Towards dynamic trot gait locomotion: Design, control, and experiments with cheetah-cub, a compliant quadruped robot. *The International Journal of Robotics Research*, 2013, **32**, 932–950.

[15] Zhang J, Gao F, Han X, Chen X, Han X. Trot gait design and CPG method for a quadruped robot. *Journal of Bionic Engineering*, 2012, **11**, 18–25.

[16] Wang X, Li M, Wang P, Guo W, Sun L. Bio-inspired controller for a robot cheetah with a neural mechanism controlling leg muscles. *Journal of Bionic Engineering*, 2012, **9**, 282–293.

[17] Herr H M and McMahon T A. A trotting horse model. *The International Journal of Robotics Research*, 2000, **19**, 566–581.

[18] Lee D V, Bertram J E, Todhunter R J. Acceleration and balance in trotting dogs. *The Journal of Experimental Biology*, 1999, **202**, 3565–3573.

[19] Gregersen C S, Silverton N A, Carrier D R. External Work and Potential for Elastic Storage at the Limb Joints of Running Dogs. The Journal of Experimental Biology, 1998, **201**, 3197–3210.

[20] Lee D V, Meek S G. Directionally compliant legs influence the intrinsic pitch behavior of a trotting quadruped. *Proceedings of the Royal Society B*: *Biological Sciences*, 2005, **272**, 567–572.

[21] Krasny D P, Orin D E. Evolution of a 3D gallop in a quadrupedal model with biological characteristics. *Journal of Intelligent & Robotic Systems*, 2010, **60**, 59–82.

[22] Jiang Z, Li M, Guo W. Running control of a quadruped robot in trotting gait. *IEEE Conference on Robotics*, *Automation and Mechatronics*, Qingdao, China, 2011, 171–177.

[23] Carroll A M, Lee D V, Biewener A A. Differential muscle function between muscle synergists: Long and lateral heads of the triceps in jumping and landing goats (Capra hircus), *Journal of Applied Physiology* , 2008, **105**, 1262–1273.